Reexamination of Kerker's conditions by means of the phase diagram

Jeng Yi Lee,[1] Andrey E. Miroshnichenko,[2,3] and Ray-Kuang Lee[1,4,*]

[1]*Institute of Photonics Technologies, National Tsing Hua University, Hsinchu 300, Taiwan*

[2]*Nonlinear Physics Centre, Research School of Physics and Engineering, The Australian National University, Canberra 2601, Australia*

[3]*School of Engineering and Information Technology, University of New South Wales, Canberra, Australian Capital Territory 2600, Australia*

[4]*Physics Division, National Center for Theoretical Sciences, Hsinchu 300, Taiwan*

(Received 17 May 2017; published 18 October 2017)

For passive electromagnetic scatterers, we explore a variety of extreme limits on directional scattering patterns in a phase diagram, regardless of the details on the geometric configurations and material properties. By demonstrating the extinction cross sections with the power conservation intrinsically embedded in the phase diagram, we give an alternative interpretation for Kerker's first and second conditions, associated with zero backward scattering (ZBS) and nearly zero forward scattering (NZFS). Physical boundaries and limitations for these directional radiations are illustrated along with a generalized Kerker's condition with implicit parameters. By taking the dispersion relations of gold silicon core-shell nanoparticles into account, we reveal the realistic parameters to experimentally implement ZBS and NZFS at optical frequencies by means of a phase diagram.

DOI: 10.1103/PhysRevA.96.043846

I. INTRODUCTION

In 1983, Kerker *et al.* revealed that, under a proper combination of magnetic and electric dipoles of a magnetodielectric particle on the subwavelength scale, one can have an asymmetric field radiation with zero backward scattering (ZBS) or zero forward scattering (ZFS), which are known as the first and second Kerker's conditions, respectively [1]. For ZBS, the permeability μ and permittivity ϵ must have the same value, i.e., $\mu = \epsilon$; whereas for ZFS, the permittivity and permeability need to satisfy the condition $\epsilon = (4 - \mu)/(2\mu + 1)$ in the quasistatic limit. Such an asymmetric radiation in the backward or forward directions also is associated with a directional Fano resonance due to constructive or destructive interferences between the induced resonant wave to the scattered one [2,3].

Experimental realizations toward directional scattering patterns have been demonstrated with a single nanoparticle made of GaAs [4], silicon [5], or a gold nanoantenna [6]. Moreover, due to the lack of a giant magnetization in natural materials at optical wavelengths, several ways are proposed to realize anomalous asymmetric radiations, such as inducing interferences among dipole and quadrupole channels on metallic-dielectric nanoparticles [7], using gain dielectric nanoparticles to compensate inherently scattering loss in order to have a zero extinction cross section [8], using nanoparticles made of a high index of refraction optical materials [9,10], and engineering aluminum nanostructures in the shape of a pyramid to induce a magnetic dipole [11].

However, when the optical theorem is taken into consideration, an inconsistency arises because the electric scattering amplitude in the forward direction is related to the total extinction cross section [12]. That is, the ZFS implies a zero extinction cross section. The consequence of zero extinction strictly requires the zeros of absorption and scattering cross sections. As a result, ZFS is an impossible phenomenon for any noninvisible passive system. Although many studies support the trends of such asymmetrical radiation [13–18], a study on the limitation and physical boundary regardless of scattering system details is still lacking.

Recently, based on the energy conservation law, i.e., the total amount of outgoing electromagnetic power by passive objects should be the same or smaller than that of the incoming one, we propose a phase diagram to reveal all allowable scattering solutions and energy competitions among absorption and scattering powers [19]. In this paper, with the power conservation intrinsically embedded in the phase diagram, we resolved the inconsistency and related exception solution in Kerker's conditions. Moreover, we explore a variety of extreme limits on directional scattering patterns in the phase diagram, regardless of the details on the geometric configurations and material properties. For ZFS, we find that forming a perfect destructive interference for a pair of scattering coefficients by electric and magnetic dipoles is forbidden for any noninvisible system, resulting in the support of *nearly* zero forward scattering (NZFS) only. Any absorption loss will destroy the required out-of-phase conditions, leading intrinsically to a nonvanished extinction cross section. Nevertheless, for ZBS, there is no such constraint for the corresponding extinction cross section. In addition, we also reveal the existence of an additional intrinsic degree of freedom to support ZBS and NZFS.

The global and possible solutions for general scattering patterns also are discussed beyond any scattering events. The robustness of NZFS on directional scattering patterns is investigated in the phase diagram with a small variation in strength or with a small material loss. Moreover, we provide a set of permeability and permittivity with an additional intrinsic degree of freedom to support NZFS by employing the inverse design method with the phase diagram in order to design functional devices with the required optical response [19]. In particular, we consider core-shell nanostructures, made of gold in the core and silicon in the shell, as a target to realize ZBS and NZFS at optical wavelengths from 450 to 800 nm. By taking the real material dispersion relation into account, we reveal the working wavelengths to demonstrate ZBS and NZFS with the same geometric configuration. With the help of the phase

*Corresponding author: rklee@ee.nthu.edu.tw

diagram, our results not only provide a deeper understanding on light-scattering patterns, but also offer a universal way to design functional scatterers for light harvesting, metasurfaces, nanoantennas, and nanosensors.

II. PHASE DIAGRAM FOR PASSIVE SCATTERERS

We start with light illuminating on an isolated spherical object by considering a linearly $\hat{x}$-polarized electromagnetic plane wave propagating along the z direction with time evolution $e^{-i\omega t}$. By applying the spherical multipole decomposition, the scattered field can be represented with two sets of scattering coefficients a_n and b_n, which correspond to the TM and TE modes, respectively. Here, the index n is used to denote the nth-order spherical harmonic channel, and the corresponding absorption, scattering, and extinction cross sections can be derived as follows [19,20]:

$$\sigma^{\text{abs}} = \sum_{n=1}^{n=\infty} \frac{(2n+1)\lambda^2}{2\pi}(\text{Re}\{a_n\} - |a_n|^2 + \text{Re}\{b_n\} - |b_n|^2),$$

$$\sigma^{\text{scat}} = \sum_{n=1}^{n=\infty} \frac{(2n+1)\lambda^2}{2\pi}(|a_n|^2 + |b_n|^2), \quad \sigma^{\text{ext}} = \sigma^{\text{abs}} + \sigma^{\text{scat}},$$

with the wavelength of incident plane-wave λ. As a rule of thumb, the main contribution to these convergent series would be related to the size parameter, defined as $k_0 a$, where a denotes the radius of this spherical object and $k_0 = 2\pi/\lambda$ is environmental wave number.

By the Kirchhoff vector integral and asymptotic analysis, the extinction cross section can be expressed in terms of the scattered electric field in the forward direction $\theta = 0$ [21,22],

$$\sigma^{\text{ext}} = \frac{4\pi}{k_0}\text{Im}[\hat{x} \cdot \vec{f}(\theta = 0)], \tag{1}$$

here, in the radiation regime (the observer is far from the scatterers) the scattered electric field can be approximated as $\vec{E}_s \to E_0 \vec{f}(\theta,\phi)e^{ik_0 r}/r$ with the strength of incident electric-field E_0. It also is known that Eq. (1) corresponds to the optical theorem, which implies that any loss, no matter from intrinsic material loss or scattering radiation, will lead to the extinction, equivalently to the enhancement of a scattered field in the forward direction.

Due to the inherently non-negative values for σ^{abs} and σ^{scat} in passive scatterers, it is obvious that a perfect zero extinction cross section exists only when both the absorption and the scattering cross sections vanish. A zero extinction cross section represents a zero scattering electric field in the forward direction, implying that the nanoparticle produces no shadow. This simple argument suggests that for any passive scattering system only invisible bodies have no shadow, but one can embed active materials to compensate scattering loss in order to achieve a zero extinction [8].

To study directional scattering patterns in terms of spherical harmonic orders we can calculate the differential scattering cross sections in the forward ($\theta = 0$) and backward ($\theta = \pi$) directions, i.e., defined as σ^{fw} and σ^{bw}, respectively [12,20],

$$\sigma^{\text{fw}} = \frac{\lambda^2}{16\pi}\left|\sum_{n=1}^{\infty}(2n+1)(a_n + b_n)\right|^2, \tag{2}$$

$$\sigma^{\text{bw}} = \frac{\lambda^2}{16\pi}\left|\sum_{n=1}^{\infty}(-1)^n(2n+1)(b_n - a_n)\right|^2. \tag{3}$$

Here, by following the original concept from Kerker *et al.* [1] to eliminate the forward or backward scattered radiations, we have ZFS or ZBS when $\sigma^{\text{fw}} = 0$ or $\sigma^{\text{bw}} = 0$ is satisfied, respectively. Conducted from Eq. (2), clearly, one can see that the key point for cancellation in the forward scattering ($\sigma^{\text{fw}} = 0$) relies on the destructive interferences between a_n and b_n, i.e., $a_n = -b_n$, corresponding to the same magnitude and out-of-phase condition in the two scattering coefficients. As for ZBS ($\sigma^{\text{bw}} = 0$), we need to have two equal scattering coefficients in the same spherical harmonic orders, i.e., $a_n = b_n$.

Now, we turn to the phase diagram for passive electromagnetic scatterers by applying the *phasor* representation to the scattering coefficients, i.e., defining $a_n = |a_n|e^{i\,\text{Arg}(a_n)}$ and $b_n = |b_n|e^{i\,\text{Arg}(b_n)}$. As we reported in Ref. [19], the power conservation intrinsically holds for the absorption cross sections $\sigma_n^{\text{abs}(a,b)} \geqslant 0$ in each spherical harmonic order, which corresponds to the colored region shown in Fig. 1(a). In addition to the absorption cross section, one also can reveal the contour plot for the supported extinction cross section in TM or TE modes, i.e., $\sigma_n^{\text{ext}(a,b)}$ with a normalization factor of $2\pi/(2n+1)\lambda^2$. By demonstrating the extinction cross section with the power conservation intrinsically embedded in the phase diagram, one can clearly see that the region to support a zero extinction cross section just corresponds to the invisible condition, i.e., $|a_n| = |b_n| = 0$, which illustrates another manifestation of the optical theorem. This phase diagram not only reports the detail energy assignments among scattering and absorption powers, but also indicates the required phase and magnitude boundaries for all the scattering coefficients. Below, based on this phase diagram, we investigate the extreme limits on light-scattering patterns.

To satisfy Kerker's first and second conditions for extremely small magnetodielectric spheres (as the dominant terms are the lowest orders), we need to satisfy the destructive or constructive interferences between the TM and the TE modes, i.e., $a_1 = -b_1$ or $a_1 = b_1$ for ZFS or ZBS, respectively. Within the quasistatic regime, the corresponding scattering coefficients for a_1 and b_1 can be expressed in terms of the permittivity ϵ and permeability μ [12,19],

$$a_1 = \left[1 + i\frac{3\lambda^3}{2(2\pi a)^3}\frac{2+\epsilon}{\epsilon - 1}\right]^{-1}, \tag{4}$$

$$b_1 = \left[1 + i\frac{3\lambda^3}{2(2\pi a)^3}\frac{2+\mu}{\mu - 1}\right]^{-1}. \tag{5}$$

Thus, the conditions $a_1 = -b_1$ or $a_1 = b_1$ lead to the famous formula $\epsilon = (4-\mu)/(2\mu+1)$ or $\mu = \epsilon$ for ZFS or ZBS, respectively [23]. However, we want to emphasize that, as one can see in Fig. 1(a), there exists an additional implicit

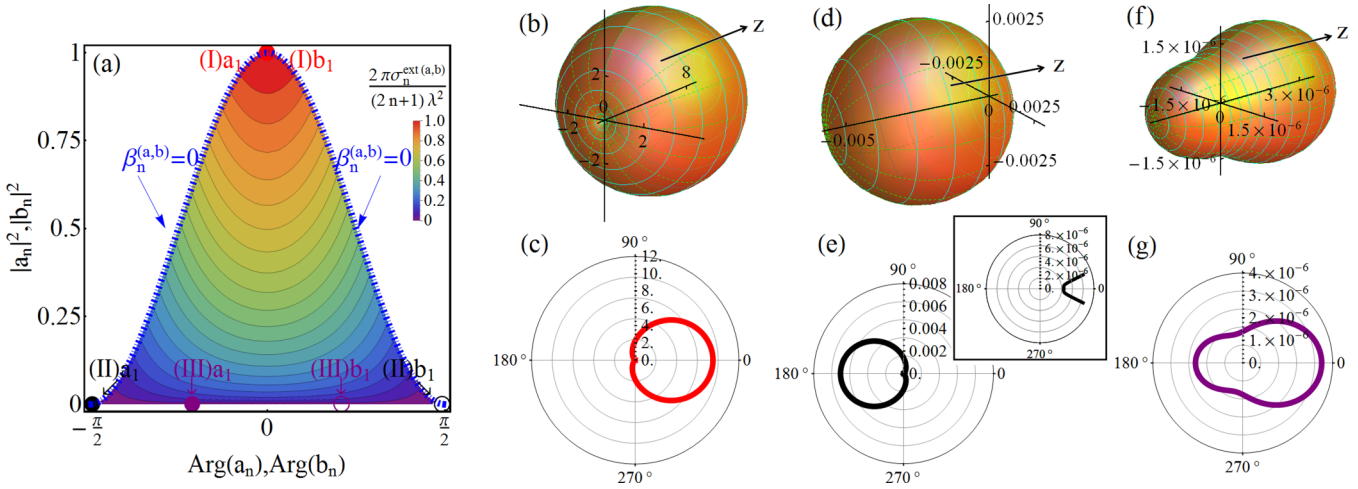

FIG. 1. (a) Phase diagram for the extinction cross section, defined by an amplitude square ($|a_n|^2$,$|b_n|^2$) and a phase [Arg(a_n),Arg(b_n)] of scattering coefficients for passive scatterers. The colored region indicates the allowed solutions with the contour line representing a constant normalized extinction cross-sectional $2\pi\sigma_n^{\mathrm{ext}(a,b)}/(2n+1)\lambda^2$ in transverse magnetic (TM) or transverse electric (TE) modes. Three sets of supported scattering states are marked as (I), (II), and (III) with the corresponding three-dimensional–two-dimensional (3D-2D) radiation patterns depicted in (b)–(g), respectively. Here, (b) and (c) reveal the ZBS condition; (d) and (e) reveal the nearly ZFS condition as a residue of scattering contributions can still be found in the enlarged window in the forward direction (see the inset); (f) and (g) reveal a state with the same extinction cross section as that of (d) and (e) (note the scale) but with losses. The size of the scatterer used in all simulations is the same by setting $a = 10^{-2}\lambda$.

degree of freedom to satisfy the destructive or constructive interferences between the TM and the TE modes. Now, to go one step further, we demonstrate how to utilize the phase diagram with this additional degree of freedom.

For the implicit parameters in the phase diagram, we introduce two real numbers $\alpha_n^{(a,b)}$ and $\beta_n^{(a,b)}$ for the nth-order spherical harmonic wave in TM and TE modes by rewriting the scattering coefficients as

$$a_n = \frac{1}{1 + i\left(\alpha_n^a + i\beta_n^a\right)}, \tag{6}$$

$$b_n = \frac{1}{1 + i\left(\alpha_n^b + i\beta_n^b\right)}. \tag{7}$$

In particular, the parameter $\beta_n^{(a,b)}$ accounts for the material lossy effects. Only when $\beta_n^{(a,b)} = 0$ is the scattering system made of lossless materials. For the allowed solutions in the phase diagram, the intrinsic power conservation automatically sets the range for these parameters, i.e., $\alpha_n^{(a,b)} = [-\infty,\infty]$ and $\beta_n^{(a,b)} = [-\infty,0]$, no matter what kind of geometric configuration or material composition for scattering systems are chosen. Also, it should be noted that the border depicted by the blue-dashed curve in Fig. 1(a) reflects a lossless boundary, i.e., $\beta_n^{(a,b)} = 0$.

To achieve ZFS, we need to have $a_1 = -b_1$. It means that a phase difference $\pm\pi$ and the same magnitude of scattering coefficients are needed. Nevertheless, as one can see from the phase diagram in Fig. 1(a), the only supported solutions are localized at [Arg(a_n) $= \pm\pi/2$, $|a_n| = 0$] and [Arg(b_n) $= \mp\pi/2$, $|b_n| = 0$]. In terms of the implicit parameters, to approach ZFS, we need to have α going to $\pm\infty$ and $\beta = 0$. Only in these asymptotic cases will the corresponding phase differences between a_1 and b_1 be $\pm\pi$ while they have the same magnitudes. The marked pair (II) corresponds to such a zero absorption and a zero scattering cross section with the extinction cross-sectional $\sigma_n^{\mathrm{ext}} = 0$. In general, the scatterer can have the same magnitude in the two lowest-order scattering coefficients $|a_1| = |b_1|$, but the required phase difference $\pm\pi$ is impossible for any noninvisible scattering system. In other words, the ideal ZFS is impossible to be realized from a passive scatterer. Only nearly zero forward scattering can be approached. Instead, to achieve ZBS, one easily can find supported solutions in the phase diagram by looking for the pair of $a_1 = b_1$. Moreover, a variety of solution pairs in the allowable region of the phase diagram can be supported.

With the help of these implicit parameters, one can generalize the Kerker's second equation as

$$\epsilon(\alpha) = \frac{3 + \alpha(k_0 a)^3}{\alpha(k_0 a)^3 - \frac{3}{2}}, \tag{8}$$

$$\mu(\alpha) = \frac{-3 + \alpha(k_0 a)^3}{\alpha(k_0 a)^3 + \frac{3}{2}}. \tag{9}$$

Here, for the simplicity, we have assumed that the scattering system is made of lossless materials, i.e., $\beta_1^a = \beta_1^b = 0$ and define $\alpha_1^a = -\alpha_1^b \equiv \alpha$ for the required condition $a_1 = -b_1$. By eliminating the implicit parameter α, one can come back to the original second Kerker's condition, i.e., $\epsilon = (4 - \mu)/(2\mu + 1)$. Based on Eqs. (8) and (9), one can expect that there exist a family of solutions to satisfy the Kerker's second condition as the implicit parameter α varies accordingly. In particular, a perfect ZFS only happens when $\alpha = \pm\infty$, which is also the condition for invisible scatterers. On the other hand, the inconsistency from the Kerker's second condition to the optical theorem can easily be interpreted in the phase diagram. As for the exception solution in the Kerker's second condition $\epsilon = \mu = -2$ [14], the corresponding implicit parameter is $\alpha = 0$. From the phase diagram, we can see that this exception

solution gives ZBS instead of ZFS. In short, the improper results conducted from the original Kerker's second condition can be resolved from this set of generalized formulas given in Eqs. (8) and (9).

Even though a perfect ZFS condition is not allowed, we can explore the possibility to minimize the forward scattering by defining the forward scattering efficiency,

$$\eta^{\mathrm{fw}} = \frac{\sigma^{\mathrm{fw}}}{\sigma^{\mathrm{scat}}}, \tag{10}$$

as the ratio between the forward scattering cross section and the total scattering cross section. For the perfect ZFS, this forward scattering efficiency goes to zero; whereas a nonzero value gives a metric to quantify the forward scattering. Then, for the lossless system $\beta_n^{(a,b)} = 0$, the forward scattering efficiency has the following form:

$$\eta^{\mathrm{fw}} = \frac{3}{4(1+\alpha^2)}. \tag{11}$$

Again, only when $\alpha \to \pm\infty$ we have the ZFS as $\eta^{\mathrm{fw}} \to 0$.

To demonstrate the supported directional radiation patterns in the phase diagram, in Figs. 1(b)–1(g), we illustrate three extreme limits on light scattering: ZBS, NZFS (with a negligible extinction cross section), and the state with the same extinction cross section as NZFS but including the material lossy effect. First, we consider the state with a maximum value in the extinction cross section, i.e., $a_1 = b_1 = 1$, which is marked as (I) in the red colors in the phase diagram of Fig. 1(a). Both the electric dipole and the magnetic dipole are at resonance, resulting in a giant scattering pattern shown in Figs. 1(b) and 1(c) for the 3D and 2D contour plots, respectively. As the $a_1 = b_1$ condition is satisfied, a clear ZBS pattern can be seen. By referring to the material properties through Eqs. (4) and (5), we have $\epsilon = -2.005$ and $\mu = -2.005$.

Next, we choose the supported solutions close to the ZFS condition, i.e., the pair marked as (II) by the black colors shown in Fig. 1(a). Clearly, from the corresponding radiation patterns shown in Figs. 1(d) and 1(e), one can see a nearly ZFS pattern but with an extremely low residue of scattering in the forward direction with the corresponding extinction cross section on the order of 10^{-6}, see the inset. By Eqs. (4) and (5), the corresponding materials can be found as $\epsilon = -2.025$ and $\mu = -1.985$. As one can see from Fig. 1(a), there exist a family of supported solutions with the same value of extinction cross sections. For example, the solution pair marked as (III) by the purple colors in Fig. 1(a) reveals the scenario with the same amount of extinction cross section as that from the solution pair (II), i.e., located on the same contour line but with the intrinsic material loss. Clearly, the out-of-phase requirement is not satisfied for the ZFS. As shown in Figs. 1(f) and 1(g), even though the strengths of the scattered electric field in the forward direction are the same as that in the solution pair (II), i.e., note the scale now is on the order of 10^{-6}, the corresponding radiation patterns in these two states are totally different. The corresponding material parameters are $\epsilon = -2.33 + 0.63i$ and $\mu = -1.61 + 0.38i$ for the state marked as pair (III). In terms of the forward scattering efficiency, for these three parameter pairs: (I), (II), and (III) chosen in Fig. 1(a), the corresponding values are $\eta^{\mathrm{fw}} = 3/4$, 0.0005, and 0.47, respectively. Again, even though the last two pairs have the same extinction cross sections, there is a big difference in their forward scattering efficiencies.

III. ROBUSTNESS OF NZFS

With the help of the phase diagram, we also can investigate the robustness of supported NZFS states by taking the strength mismatch or material lossy effects into consideration. In terms of the explicit parameters, we introduce two small perturbation terms $\delta\alpha$ and $\delta\beta$ into the scattering coefficient a_1, i.e., $a_1 = [1 + i(\alpha + \delta\alpha + i\delta\beta)]^{-1}$. In Fig. 2(a), we illustrate the perturbed solutions in the phase diagram with the unperturbed one, marked as (I). Specifically, a perturbation with $\delta\alpha = 0$, $\delta\beta = -1$, marked as (II), moves the unperturbed state ($\alpha = 20$) away from the lossless boarder, i.e., to the right-hand side; whereas a perturbation with $\delta\alpha = \pm 1$, $\delta\beta = 0$ moves the original state downward or upward along the lossless trajectory, i.e., to the markers (III) or (IV), respectively.

To illustrate the scattering patterns with small perturbations, we can expand the required ZFS condition $a_1 + b_1 = 2/(1+\alpha^2)$ to the first-order terms of $\delta\alpha$ and $\delta\beta$. That is

$$a_1 + b_1 \approx \frac{2 - \delta\beta - i\delta\alpha}{1+\alpha^2}, \tag{12}$$

here $\delta\beta$ is a negative value to account for the material losses. Then, in the auxiliary complex space for $a_1 + b_1$ as shown in Fig. 2(b), one can see clearly that the amplitude of $a_1 + b_1$ should be kept as small as possible in order to have an optimized NZFS. When $\delta\alpha = 0$ but $\delta\beta \neq 0$, Eq. (12) can be reduced to $a_1 + b_1 \approx (2 - \delta\beta)(1+\alpha^2)^{-1}$, which represents the induced forward scattering due to material loss with an additional incremental amplitude $(-\delta\beta)(1+\alpha^2)^{-1}$. On the other hand, when $\delta\beta = 0$ but $\delta\alpha \neq 0$, Eq. (12) becomes $a_1 + b_1 \approx (2 - i\delta\alpha)(1+\alpha^2)^{-1}$, which gives an extra contribution in the forward scattering by $(\pm\delta\alpha)(1+\alpha^2)^{-1}$. With the increments in amplitude or phase from the perturbed solutions, we plot the resulting scattering patterns in Fig. 2(c) and its enlarged ones in Fig. 2(d). As one can see, the material lossy effect from a nonzero $\delta\beta$ significantly deteriorates the NZFS. Nevertheless, with $\delta\alpha \neq 0$ but $\delta\beta = 0$, the NZFS states is more insensitive to a mismatch in magnitudes only [24]. Again, these examples indicate that the NZFS state relies not only on the perfect match in strengths between a_1 and b_1, but also much crucially on the phase difference.

IV. CORE-SHELL PARTICLES

In addition to the isotropic and homogeneous single-layered spherical scatterers, to realize directional scattering patterns, such as NZFS or ZBS, we apply our phase diagram for core-shell particles, which recently are readily accessible with the experimental advance [25]. To realize such kinds of a core-shell configuration, one may use the self-sacrificing template method to synthesize highly uniform nanoparticles with a tunable thickness [26,27]. In particular, we consider a core-shell nanoparticle with gold in the core and silicon in the shell as shown in the inset of Fig. 3. When realistic geometric size is taken for implementation, we set the outer radius r to be 64 nm for the whole scatterer and the core radius r_c to be

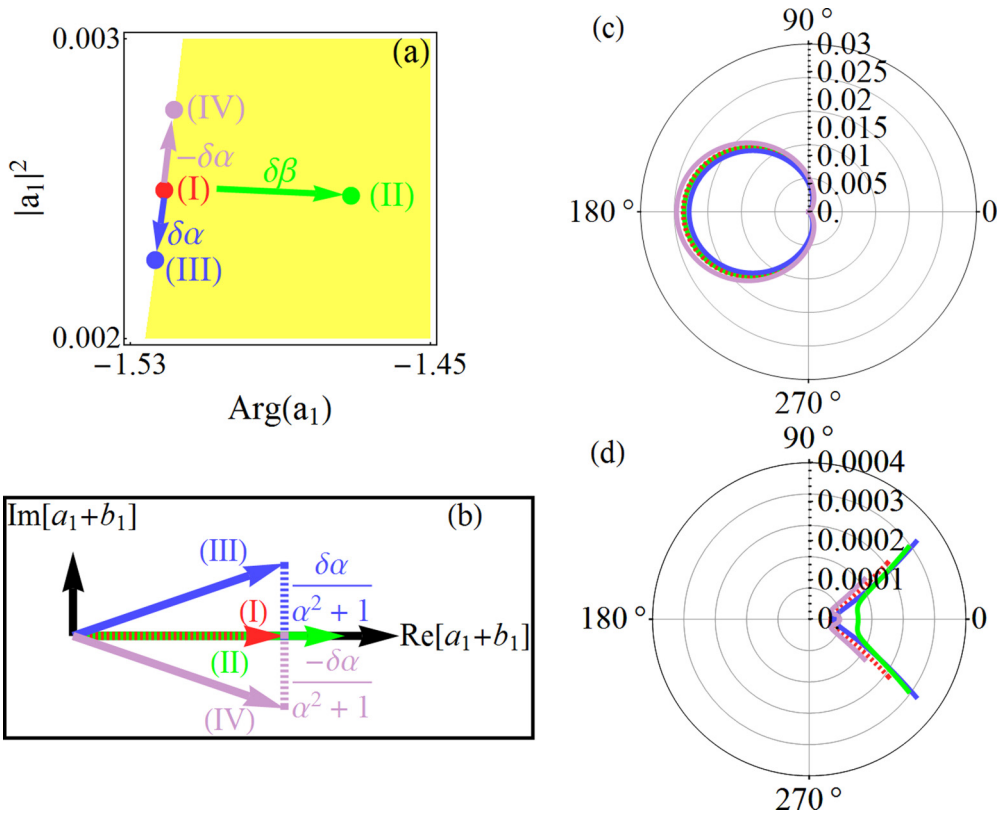

FIG. 2. (a) An unperturbed NZFS state marked as (I) in the phase diagram is studied with the introduction of a small perturbation of $\delta\beta$ as marker (II), $\delta\alpha$ as marker (III), and $-\delta\alpha$ as marker (IV), respectively. (b) The corresponding auxiliary complex space, defined by the real and imaginary parts of the scattering coefficient $a_1 + b_1$ for the unperturbed and perturbed states. (c) The resulting 2D scattering patterns for the unperturbed and perturbed states given in (a) with the enlarged window in the forward direction shown in (d).

12 nm for the inner gold particle [25]. Moreover, for the optical wavelength region, i.e., $\lambda = 450$–800 nm, the corresponding material dispersion data also are taken into consideration from the experimental data [28].

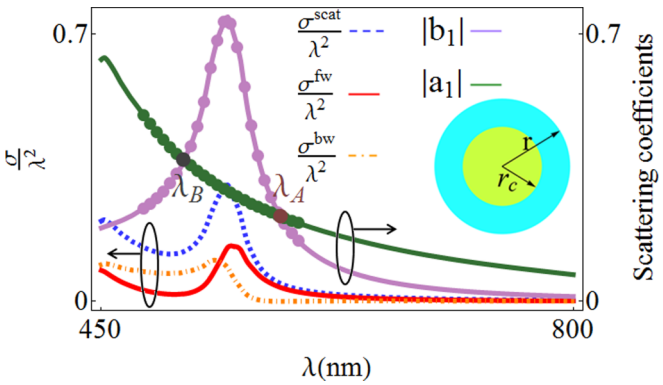

FIG. 3. The corresponding spectra for the scattering cross section (the dashed-blue curve), the forward scattering cross section (the solid-red curve), the backward scattering cross section (the dashed-dotted-orange curve), and the absolute values of the two lowest-order scattering coefficients ($|a_1|$ and $|b_1|$ in the green and purple colors, respectively) for a core-shell nanoparticle shown in the inset. This core-shell particle consists of gold in the core and silicon in the shell with the corresponding dispersion relation taken from the experimental data [28].

Based on the dispersion relations for gold and silicon in Fig. 3 we also depict the corresponding total, forward, and backward scattering cross sections σ^{scat}, σ^{fw}, and σ^{bw} (normalized to λ^2) in the dashed-blue, solid-red, and dashed-dotted-orange colors, respectively. Due to the normal mode resonance from the TM mode, there exists a resonance peak around 550 nm. In order to give an illustration on the scattering behavior, in the same plot, the magnitudes of two lowest-order scattering coefficients $|a_1|$ and $|b_1|$ also are depicted in the green and purple colors, respectively. One can see clearly that, in the long-wavelength limit, i.e., the incident wavelength $\lambda > 600$ nm, the electric dipole is always dominant, i.e., $|a_1| > |b_1|$. However, near the resonance region, around $\lambda = 550$ nm, the magnetic dipole can overwhelm the electric one, i.e., $|b_1| > |a_1|$. When we approach the resonance condition by decreasing the wavelength, there exist two crossing points, marked as $\lambda_A = 583$ and $\lambda_B = 511$ nm in Fig. 3, having the same magnitude in the two scattering coefficients.

Even though with the help of the spectra in Fig. 3 we can expect to have exotic light scattering at the two crossing points, the underlying physical picture to support ZBS or ZFS is not clear. Instead, to have a better understanding of the scattering properties for such a core-shell configuration, in Fig. 4(a), we plot all the trajectories at different wavelengths in the phase diagram. As the wavelength decreases (from a long wavelength to a short wavelength), i.e., indicated by the arrows, these two lowest-order scattering coefficients move within the supported region. First of all, in the long-wavelength limit, both a_1 and

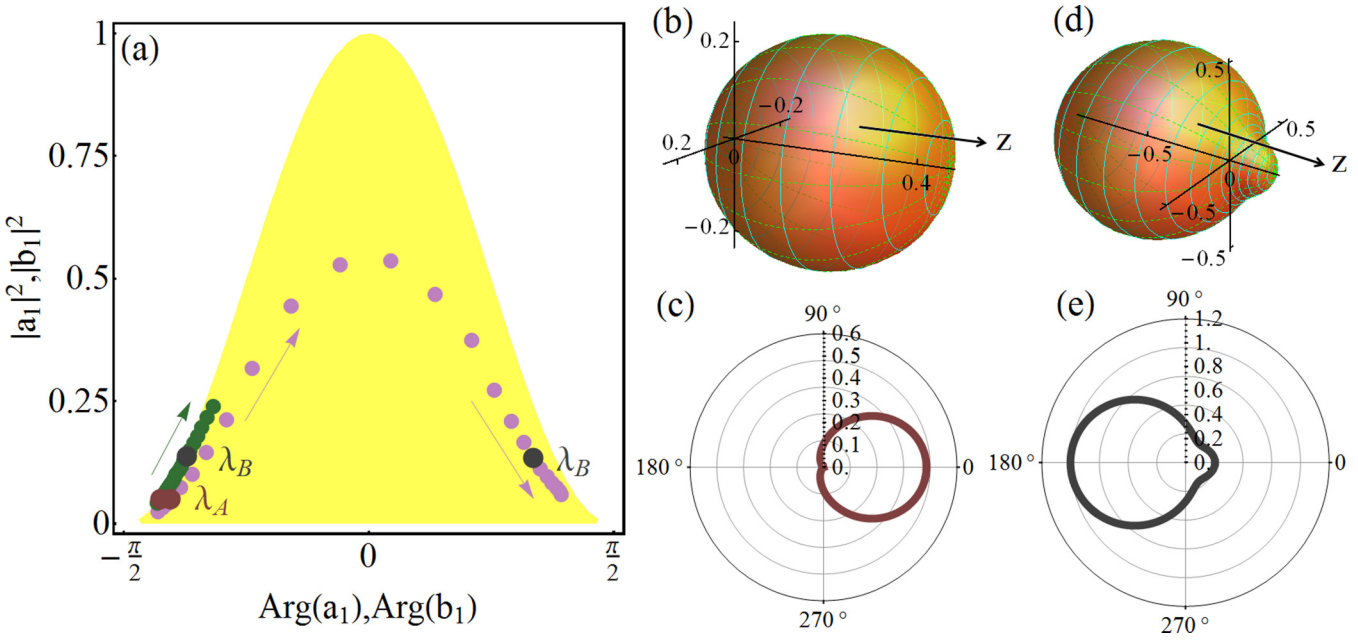

FIG. 4. Locations of the two lowest-order scattering coefficients a_1 and b_1 at different wavelengths in the phase diagram, generated from the data points depicted in Fig. 3. Here, the green and purple dots represent the scattering coefficients for electric and magnetic dipoles a_1 and b_1, respectively. The markers λ_A and λ_B highlight the two crossing points marked in Fig. 3, i.e., for the ZBS and NZFS conditions, respectively. The corresponding 3D-2D scattering patterns are plotted in (b) and (c) for the ZBS condition (marker λ_A) and in (d) and (e) for the NFZS condition (marker λ_B).

b_1 are located at the same (left) side in the phase diagram, i.e., near the phase $-\pi/2$. Then, as the wavelength decreases, they meet together at the crossing point λ_A, indicating the relative phase between them is 0. Now, we have $a_1 = b_1$. The resulting scattering patterns at this crossing point λ_A is ZBS as clearly demonstrated in Figs. 4(b) and 4(c) for the 3D and 2D plots, respectively.

On the other hand, due to the magnetic dipole resonance, the trajectory for the scattering coefficient b_1 should pass through the center [Arg(b_1) = 0] in the phase diagram. However, for the scattering coefficient a_1, it would stay on the same (left) side as long as the electric dipole resonance is not excited. Then, we have the possibility to generate the second crossing point at λ_B at which the scattering coefficients a_1 and b_1 form a complex conjugated pair in the phase diagram. As we discussed above, now we have $|a_1| = |b_1|$, but the phase difference is not large enough to meet the out-of-phase shift. The resulting radiation pattern can be expected to be a NZFS only as shown in Figs. 4(d) and 4(e). In this practical example, we have the forward scattering efficiency $\eta^{\mathrm{fw}} = 0.15$.

With the core-shell nanoparticle illustrated above, we demonstrate a direct interpretation of the directional scattering patterns through the supported trajectories in the phase diagram. In particular, by varying the incident light wavelength, we predict having a significant change in the directional scattering patterns, i.e., from ZBS to NZFS with a single configuration. Although our discussion is limited only to spherical structures, the concept and approach here can be applied easily to other nonspherical geometries. In addition to the lowest orders, one also can take higher-order spherical harmonic channels into consideration as a general extension. Moreover, we should stress that the origin of our phase diagram comes from the plane-wave illumination on a spherical structure of the scattering obstacle. For other wave-front illuminations or different structures, the magnetic quantum number m should need to be considered. However, the multipole expansion is independent of the type in incident excitations. That is, any incident field can be decomposed into a series of multipoles. Different excitations will be described by different series. But, each multipole contribution will be exactly the same, regardless of the overall series.

V. CONCLUSION

To summarize, with the supported solutions in the phase diagram, we revisit Kerker's first and second conditions on the ZBS and ZFS. In addition to the explanations on the scattering coefficients, we give a clear physical picture on the physical bounds for the scattering distributions. The known problems with the inconsistency and related exception solutions in the original Kerker's second condition can be resolved by means of the phase diagram. We also reveal that there exist a set of implicit parameters (α and β) to compose the scattering coefficients and derive a generalized Kerker's condition. In the phase diagram, a perfect ZFS requires the asymptotic conditions as the implicit parameter α goes to $\pm\infty$. To be consistent with the optical theorem, only NZFS can be realized for passive electromagnetic scatterers with a finite value of the implicit parameter α. The robustness of NZFS also is investigated in the phase diagram with a small variation in the scattering strength or with material losses. To implement NZFS and ZBS, a core-shell nanoparticle is proposed with the real material dispersion relation taken into consideration. Through the supported trajectories in the phase diagram, we

predict a change from ZBS to NZFS in the scattering patterns with the same geometric configuration but just decreasing the incident wavelength in the optical domain. With the advances in nanoparticle syntheses, these extreme limits on directional scattering readily can promote the designs on nanodevices.

ACKNOWLEDGMENT

This work was supported, in part, by the Ministry of Science and Technology, Taiwan, under Contract No. 105-2628-M-007-003-MY4, and by the Australian Research Council.

[1] M. Kerker, D.-S. Wang, and C. L. Giles, Electromagnetic scattering by magnetic spheres, J. Opt. Soc. Am. **73**, 765 (1983).

[2] A. E. Miroshnichenko, S. Flach, and Y. S. Kivshar, Fano resonances in nanoscale structures, Rev. Mod. Phys. **82**, 2257 (2010).

[3] M. I. Tribelsky, S. Flach, A. E. Miroshnichenko, A. V. Gorbach, and Y. S. Kivshar, Light Scattering by a Finite Obstacle and Fano Resonances, Phys. Rev. Lett. **100**, 043903 (2008).

[4] S. Person, M. Jain, Z. Lapin, J. J. Sáenz, G. Wicks, and L. Novotny, Demonstration of zero optical backscattering from single nanoparticles, Nano Lett. **13**, 1806 (2013).

[5] Y. H. Fu, A. I. Kuznetsov, A. E. Miroshnichenko, Y. F. Yu, and B. Luk'yanchuk, Directional visible light scattering by silicon nanoparticles, Nat. Commun. **4**, 1527 (2013).

[6] R. Alaee, R. Filter, D. Lehr, F. Lederer, and C. Rockstuhl, A generalized kerker condition for highly directive nanoantennas, Opt. Lett. **40**, 2645 (2015).

[7] Y. Li, M. Wan, W. Wu, Z. Chen, P. Zhan, and Z. Wang, Broadband zero-backward and near-zero-forward scattering by metallo-dielectric core-shell nanoparticles, Sci. Rep. **5**, 12491 (2015).

[8] Y.-M. Xie, W. Tan, and Z.-G. Wang, Anomalous forward scattering of dielectric gain nanoparticles, Opt. Express **23**, 2091 (2015).

[9] A. I. Kuznetsov, A. E. Miroshnichenko, Y. H. Fu, J. Zhang, and B. Luk'yanchuk, Magnetic light, Sci. Rep. **2**, 492 (2012).

[10] A. I. Kuznetsov, A. E. Miroshnichenko, M. Brongersma, Y. S. Kivshar, and B. Luk'yanchuk, Optically resonant dielectric nanostructures, Science **354**, 2472 (2016).

[11] S. R. K. Rodriguez, F. B. Arango, T. P. Steinbusch, M. A. Verschuuren, A. F. Koenderink, and J. G. Rivas, Breaking the Symmetry of Forward-Backward Light Emission with Localized and Collective Magnetoelectric Resonances in Arrays of Pyramid-Shaped Aluminum Nanoparticles, Phys. Rev. Lett. **113**, 247401 (2014).

[12] A. Alú and N. Engheta, How does zero forward-scattering in magnetodielectric nanoparticles comply with the optical theorem? J. Nanophoton. **4**, 041590 (2010).

[13] R. V. Mehta, R. Patel, R. Desai, R. V. Upadhyay, and K. Parekh, Experimental Evidence of Zero Forward Scattering by Magnetic Spheres, Phys. Rev. Lett. **96**, 127402 (2006).

[14] B. G. Cámara, F. González, F. Moreno, and J. M. Saiz, Exception for the zero-forward-scattering theory, J. Opt. Soc. Am. A **25**, 2875 (2008).

[15] J. M. Geffrin, B. C. Cámara, R. G. Medina, P. Albella, L. S. F. Pérez, C. Eyraud, A. Litman, R. Vaillon, F. González, M. N. Vesperinas, J. J. Sáenz, and F. Moreno, Magnetic and electric coherence in forward- and back-scattered electromagnetic waves by a single dielectric subwavelength sphere, Nat. Commun. **3**, 1171 (2012).

[16] W. Liu, A. E. Miroshnichenko, D. N. Neshev, and Y. S. Kivshar, Broadband unidirectional scattering by magneto-electric core-shell nanoparticles, ACS Nano **6**, 5489 (2012).

[17] I. Staude, A. E. Miroshnichenko, M. Decker, N. T. Fofang, S. Liu, E. Gonzales, J. Dominguez, T. S. Luk, D. N. Neshev, I. Brener, and Y. S. Kivshar, Tailoring directional scattering through magnetic and electric resonances in subwavelength silicon nanodisks, ACS Nano **7**, 7824 (2013).

[18] J. Yan, P. Liu, Z. Lin, H. Wang, H. Chen, C. Wang, and G. Yang, Directional fano resonance in a silicon nanosphere dimer, ACS Nano **9**, 2968 (2015).

[19] J. Y. Lee and R.-K. Lee, Phase diagram for passive electromagnetic scatterers, Opt. Express **24**, 6480 (2016).

[20] C. F. Bohren and D. R. Huffman, *Absorption and Scattering of Light by Small Particles* (Wiley, New York, 1998).

[21] J. D. Jackson, *Classical Electrodynamics* (Wiley, New York, 1975).

[22] R. G. Newton, Optical theorem and beyond, Am. J. Phys. **44**, 639 (1976).

[23] On the extremely subwavelength scale $\lambda^3/a^3 \gg 1$, Kerker *et al.* neglected the real part of the denominator in Eqs. (4) and (5), resulting in the Kerker's second condition. However, such an approximation violates the power conservation.

[24] It should be noted that a small variation in $\delta\alpha$ also changes the phase slightly. But this phase change is smaller than that induced by the mismatch in magnitudes.

[25] R. G. Chaudhuri and S. Paria, Core/Shell nanoparticles: Classes, properties, synthesis mechanisms, characterization, and applications, Chem. Rev. **112**, 2373 (2011).

[26] M.-C. Tsai, J.-Y. Lee, P.-C. Chen, Y.-W. Chang, Y.-C. Chang, M.-H. Yang, H.-T. Chiu, I.-N. Lin, R.-K. Lee, and C.-Y. Lee, Effects of size and shell thickness of TiO_2 hierarchical hollow spheres on photocatalytic behavior: an experimental and theoretical study, Appl. Catal. B **147**, 499 (2014).

[27] J.-Y. Lee, M.-C. Tsai, P.-C Chen, T.-T. Chen, K.-L. Chan, C.-Y. Lee, and R.-K. Lee, Thickness effect on light absorption and scattering for nanoparticles in the shape of hollow spheres, J. Phys. Chem. C **119**, 25754 (2015).

[28] E. D. Palik, *Handbook of Optical Constants of Solids* (Academic Press, New York, 1985).